Atmos. Chem. Phys. Discuss., 13, 32269–32289, 2013
www.atmos-chem-phys-discuss.net/13/32269/2013/
doi:10.5194/acpd-13-32269-2013

Atmospheric Chemistry and Physics Discussions

Biomass burning aerosol properties over the Northern Great Plains during the 2012 warm season

T. Logan[1], **B. Xi**[1], **and X. Dong**[1,2]

[1]University of North Dakota, Grand Forks, ND, USA
[2]GCESS, Beijing Normal University, Beijing, China

Received: 8 October 2013 – Accepted: 25 November 2013 – Published: 10 December 2013

Correspondence to: X. Dong (dong@aero.und.edu)

Published by Copernicus Publications on behalf of the European Geosciences Union.

Abstract

Biomass burning aerosols can have a large impact on atmospheric processes as well as human health. During the 2012 warm season, a large outbreak of wildfires originating from the intermountain and Pacific states provided many opportunities to observe the physical and chemical properties of biomass smoke aerosols. Six biomass burning smoke plumes (26 June–15 September) have been observed by the newly installed Grand Forks, North Dakota, AERONET site (47.91° N, 97.32° W) and are selected for this study. To identify the source regions, HYSPLIT backward trajectory model data and satellite imagery are used to track these events. The volume size distribution and spectral aerosol optical depth (AOD) dependence showed the relative influences of fine and coarse mode particles. Case II (4 July) had the strongest fine mode influence as evidenced by a strong spectral AOD dependence while Case VI (15 September) had the strongest coarse mode influence with the weakest spectral dependence. The spectral dependences of absorption aerosol optical depth (AAOD) and single scattering co-albedo (ω_{oabs}) illustrated the varying absorption of the smoke plumes by inferring the relative contributions of strongly and weakly absorbing carbonaceous species. More specifically, the AAOD parameter is primarily influenced by aerosol particle size while ω_{oabs} is more dependent on aerosol composition. The AAOD spectral dependences for Cases I (26 June), III (31 July), and VI were weaker than those from Cases II, IV (28 August), and V (30 August). However, the spectral ω_{oabs} dependences were different in that the smoke particles in Cases III and VI had the strongest absorption while Cases I, II, IV, and V had moderate to weakly absorbing particles. In addition, a weak correlation was found between plume transport time and particle absorption where strongly absorbing carbon was converted to weakly absorbing carbon.

ACPD
13, 32269–32289, 2013

1 Introduction

Dry conditions during an exceptionally mild winter and warm spring led to an outbreak of wildfires in many areas of North America including the intermountain and Pacific states in the United States. Over 5 million acres nationwide had been burned in the first nine months of 2012 (http://www.nifc.gov/fireInfo/nfn.htm). As a result of the fires, numerous smoke plumes were observed several hundreds to thousands of kilometers away from their combustion sources and also affected the air quality in the areas along the transport route (EPA, www.airnow.gov). In late June, biomass smoke plumes were observed in the northern Great Plains region for the first time and monitored by the newly installed Grand Forks Aerosol Robotic Network (AERONET) site. Before the installation of this site (October 2011), there were few active ground-based observation stations between the intermountain west and the eastern United States.

Many recent studies have illustrated the impact of biomass burning aerosols on not only climate, but also air quality and human health (Li et al., 2011; Ramanathan et al., 2001; Pope et al., 2004). Air quality downwind of the wildfires deteriorates due to the generation of particulate matter (PM), ozone (O_3), and nitrogen oxides (NO_x) from the reaction between sunlight and organic compounds present in the biomass smoke (Jimenez et al., 2009; Adler et al., 2011; McKendry et al., 2011; Jacobson et al., 2012). In fact, air quality monitoring stations often observe an increase in PM and O_3 within a matter of hours to days, depending on the synoptic weather pattern and distance between the fire and monitoring stations. Biomass smoke plumes occasionally mix with ambient pollution (in the case of large urban/industrial areas) creating an increased risk for populations susceptible to cardio-pulmonary ailments (e.g., young children and the elderly) (Jimenez et al., 2009; Pope et al., 2004).

Biomass smoke aerosols account for 40–60 % of all tropospheric carbonaceous aerosols and are capable of absorbing and scattering incoming solar radiation (Adler et al., 2011; Ramanathan et al., 2001; Kondo et al., 2011). Black carbon (BC) and organic carbon (OC) compounds are the primary constituents of biomass smoke where

ACPD
13, 32269–32289, 2013

OC can represent thousands of chemically reactive volatile and semi-volatile carbon species (e.g. brown carbon, secondary organic aerosols) (Lewis et al., 2008; Jacobson, 2012; Zaveri et al., 2012). BC absorbs solar photons across much of the E-M spectrum while OC is strongly absorbing in the shortwave and weakly absorbs in the near IR (Ramanathan et al., 2001; Jacobson, 2012).

The chemical and physical nature of biomass smoke aerosols depend on their mode of generation (Lewis et al., 2008; Reid and Hobbs, 1998; Reid et al., 1998). The formation of biomass smoke is highly complex due to the wide variety of combustion temperatures which represent either a "flaming" or "smoldering" combustion phase (Reid and Hobbs, 1998; Reid et al., 1998, 2005; Jacobson, 2012). In general, the flaming phase creates particles with BC cores (e.g. soot) along with OC compounds that condense onto the cores creating a coating while the smoldering phase tends to produce less BC and more OC in the vapor form which can eventually form new particles through condensation (Reid and Hobbs, 1998; Reid et al., 1998, 2005; Lack and Cappa, 2010; Zaveri et al., 2012). These coatings can either enhance or diminish the absorption of biomass particles which creates uncertainty when modeling their optical and chemical properties (Reid et al., 2005; Lack and Cappa, 2010; Andreae and Gelencsér, 2006).

This study identified biomass burning smoke source regions and transport routes and inferred the physical and chemical properties of six biomass burning aerosol plumes cases during the 2012 North American warm season (26 June–15 September). In particular, we focused on the observations made by the newly operational Grand Forks, North Dakota, AERONET ground-based site. A brief discussion of AERONET, the aerosol parameters retrieved by AERONET, and a particle trajectory model used to track the origins of the smokes plumes are given in Sect. 2. The analysis and discussion of six smoke plumes as observed by Grand Forks are presented in Sect. 3. The final section includes a brief summary and future work.

ACPD
13, 32269–32289, 2013

2 Methodology

2.1 AERONET

The AErosol RObotic NETwork (AERONET) consists of CIMEL sun/sky radiometers placed in a world-wide framework of observation stations (Holben et al., 1998) capable of retrieving aerosol optical products at discrete wavelengths ranging from 440 nm (visible) to 1020 nm (near IR) (Schuster et al., 2006; Eck et al., 2005). This study used Level 2 data products (cloud screened, quality assured) with AOD_{440} greater than 0.4 to ensure a high degree of accuracy (Dubovik et al., 2002). The aerosol products were generated using inversion techniques developed by Dubovik and King (2000) and Dubovik et al. (2000), and quality assurance using Holben et al. (2006).

The AERONET products analyzed in this study include both hourly and daily mean extinction and absorption aerosol optical depths (AOD and AAOD) which are used to calculate the single scattering co-albedo (henceforth known as ω_{oabs}). AOD is a measure of the total column extinction of light due to aerosols and is the sum of the scattering and absorption optical depths. The Angström exponent (α) is the negative log-slope derivative of AOD and can discern coarse and fine mode influences of a group of particles (Schuster et al., 2006; Gobbi et al., 2007; Bergstrom et al., 2007). Large α values (> 0.75) denote fine mode particles while small values (≤ 0.75) denote particles in the coarse mode (Reid et al., 1998; Gobbi et al., 2007; Logan et al., 2013). Likewise, the absorption Angström exponent (α_{abs}) is the negative log-slope derivative of AAOD and can discern aerosol composition and type (Russell et al., 2010; Bergstrom et al., 2007; Logan et al., 2013). For example, mineral dust is strongly absorbing in the shortwave and typically has higher α_{abs} values than pollution and biomass burning aerosols (e.g., Russell et al., 2010; Bergstrom et al., 2007; Logan et al., 2013). Aerosols dominated by black carbon (BC) have α_{abs} values of 1–2 while aerosols dominated by organic carbon (OC) can have values that exceed 2 (Logan et al., 2013; Bergstrom et al., 2007; Russell et al., 2010). In the case of aerosol mixtures, this parameter will be difficult to use to identify aerosol types (Logan et al., 2013). The ω_{oabs} parameter, defined as

ACPD
13, 32269–32289, 2013

the ratio of AAOD to AOD, illustrates the absorbing capacity of aerosols and can give clues to their carbonaceous content which have been known to change during transport due to photochemical reactions, humidity and other physical/chemical processes (Arola et al., 2011; Corr et al., 2012; Jacobson, 2012; Logan et al., 2013). As a result the spectral dependences of AOD, AAOD, and ω_{oabs} are used to investigate possible correlations between biomass burning smoke regions, transport, and carbonaceous content. A summary of the retrievals of these parameters is found in Table 1.

2.2 HYSPLIT

The Hybrid Single Particle Lagrangian Integrated Trajectory Model (HYSPLIT) computes the advection of a single pollutant particle trajectory by assuming a dispersion rate (Draxler and Hess, 1997, 1998; Draxler 1999; Draxler and Rolph, 2012; Rolph, 2012). Model inputs include: trajectory (forward or backward), location of particles (latitude/longitude), model time span, time of model initiation (UTC time), and particle height (a.g.l. in meters). This study will use 84 h backward trajectories as smoke plumes were usually observed over Grand Forks within 1–3 days of a wildfire incident during periods of favorable meteorological conditions (i.e., high pressure ridges and wind patterns). The typical heights of the smoke layers rarely exceeded 5 km and were confined either close to or within the planetary boundary layer (Robock, 1988).

3 Results and discussion

3.1 Warm season over Grand Forks

Figure 1 shows a time series of the hourly mean AOD_{440} along with the six selected cases of smoke plumes over the Grand Forks AERONET site (47.91° N, 97.32° W) during the warm season of 2012. Each peak in AOD_{440} is followed by a sharp decrease which denotes the passage of either a short wave trough or low pressure system that removed much of the smoke from the area (i.e., clouds or precipitation) or a shift in

ACPD
13, 32269–32289, 2013

wind direction (from southerly to westerly). This pattern repeated itself throughout the summer and early autumn until the fires were eventually extinguished. Therefore, it is apparent that the observed AOD_{440} values at Grand Forks depended not only on their original source regions, but also on their transport pathway from the source regions to Grand Forks.

To identify the source regions of the six cases in Fig. 1, the HYSPLIT backward trajectory model was used to track the origins of the smoke plumes at the 3 km level (Fig. 2). The locations of major fires along their trajectory routes were also displayed. In general, the backward trajectories revealed source regions in three parts of the United States: the intermountain west states (Colorado and Wyoming), northern Rockies (Montana and Idaho), and the Pacific states (Washington, Oregon, and California). Note that fires that lie outside of the trajectory path generated smoke plumes that were eventually advected in the general direction of each trajectory to the vicinity of Grand Forks.

The trajectories are marked every 24 h in order to show the temporal movement of the smoke plumes from the source regions to Grand Forks. Cases II, III, and V had the fastest transport times ($\leq$ 1 day). Case VI had a transport time of nearly 36 h while Cases I and IV had the slowest transport times that approached 3 days. Note that any smoke plumes within the periphery of the ridge traveled faster than those smoke plumes that are closer to the center of the high pressure. Based on the archived meteorological observations and model data, high pressure ridges were determined as the primary processes responsible for transporting smoke plumes (www.esrl.noaa.gov/psd/data/composites/day/). Figure 3a–c shows the locations of the wildfire source regions for Cases III, V, and VI while Fig. 3d–f shows evidence of the smoke plumes over Grand Forks. These cases exhibit vastly different optical properties from the other cases and will be further discussed in the next section.

ACPD
13, 32269–32289, 2013

3.2 Biomass smoke plume optical properties

Figure 4a shows the particle volume size distribution for the six cases. Case II had the strongest fine mode influence (with little coarse mode influence) while Case VI had the strongest coarse mode influence. It is evident that the aerosols had undergone some degree of coagulation and/or hygroscopic growth during transport since all cases exhibited a bimodal distribution. In Fig. 4b, the AOD spectral variations highly depend on their size distributions and fit the typical range of biomass burning aerosols (Chung et al., 2012; Logan et al., 2013). For example, Case V had the strongest AOD spectral dependence and therefore the highest α value (1.98) while Cases I and VI had the weakest dependence with lower values of 1.54 and 1.55, respectively. Though it is not surprising that Cases I and VI had the lowest α values due to a stronger coarse mode influence (Fig. 4a), it is surprising that Case V had higher α than Case II. This is likely due to more coagulation of the smoke particles during transport for Case V than for Case II and thus warrants further study.

3.2.1 Biomass smoke plume physico-chemical properties

First we note that the exact contributions of the black and organic carbon constituents to the spectral dependences of AAOD and ω_{oabs} are difficult if not impossible to determine solely from AERONET or any platform that does not involve chemical spectroscopy (e.g., thermal denuder, mass spectrometer, etc.). This issue is complicated even further by the fact that smoke particles from the flaming combustion phase can have vastly different physico-chemical properties than particles from the smoldering phase. However, previous studies have reported the relative black and organic carbon proportions of smoke plumes from moments after pyrolysis to hours and days during transport and concluded: (a) absorption of the smoke particles does decrease over time and (b) the flaming combustion phase produces more strongly absorbing organic compounds than the smoldering phase (Martins et al., 1998a, b; Reid et al., 1998; Corr

ACPD
13, 32269–32289, 2013

et al., 2012). Hence, this study used the spectral dependences of AAOD and ω_{oabs} as a means to apply these conclusions to the six cases.

Figure 4c and d shows the spectral dependences of AAOD and ω_{oabs}. All cases had a normalized AAOD dependence of 0.4–0.5 which is typical for biomass burning aerosols (Chung et al., 2012; Logan et al., 2013). Similar to Fig. 4b, Case VI had the weakest AAOD spectral dependence while Case V had the strongest. Case VI was previously identified as having a strong coarse mode influence. The larger particles tended to scatter more than they absorb (especially at the longer wavelengths), thus the weaker AAOD spectral dependence. Cases I and III had relatively weak dependences that could also be attributed to their strong coarse mode contributions. Conversely, Cases II, IV, and V had the stronger AAOD spectral dependences since the fine mode particles in turn exhibited more absorption at the longer wavelengths due to their size.

Organic carbon (OC) compounds in the smoke particles are responsible for the strong absorption in the visible while black carbon (BC) influences the absorption in the near IR. Figure 4d shows that Case V had the lowest overall ω_{oabs} values, suggesting that though the fine mode particles have a large degree of extrinsic absorption, the carbonaceous compounds themselves are weakly absorbing. However, the slight increase in spectral ω_{oabs} with wavelength does indicate a small BC influence. Since this plume arrived at Grand Forks within 24 h, the amount of weakly absorbing OC cannot be explained by chemical reactions alone but may be a result of smoke plumes that were generated from the low temperature "smoldering phase" (Reid et al., 1998; Martins et al., 1998b). Case II consisted of the smoke plume with the strongest fine mode influence and had nearly the same ω_{oabs} values as Case V but with lesser coarse mode influence. This suggests that a smaller amount of coagulation and/or hygroscopic growth may have occurred during transport for Case II.

Case III had the highest spectral ω_{oabs} values which increase with wavelength denoting strongly absorbing carbonaceous influences (BC and OC). The plume (transit time of 24 h) was generated by a fresh wildfire which would explain the large amount of absorption (Martins et al., 1998b). In addition, the α_{abs} value for this case is 1.07

ACPD
13, 32269–32289, 2013

which is close to the theoretical value of unity for submicron BC. Case VI had the second highest spectral ω_{oabs} values that increase with increasing wavelength denoting strongly absorbing BC and OC in addition to having a strong coarse mode influence. This is likely a result of the combination of fresh smoke from the Pacific Northwest wildfires (WA and OR) in addition to smoke from ongoing fires in central Idaho (since early August) (see Fig. 3). Though Bergstrom et al. (2007) pointed out that the single scattering albedo (ω_o) is a function of both size and composition, this case showed how the ω_{oabs} parameter (1-ω_o) captured more of the internal composition of the smoke particles than the AAOD parameter (Logan et al., 2013).

Cases I and IV had smoke plumes that took the longest time to advect from their source regions to Grand Forks (~ 3 days). Both cases featured moderate overall ω_{oabs} spectral dependences with Case I having a slightly lower absorption. This also correlated with the stronger coarse mode influence than Case IV possibly indicating that more coagulation may have taken place during transport in Case I than Case IV. It should be noted that given the time it took for the smoke plumes to reach Grand Forks, some conversion of strongly to weakly absorbing organic carbon may have taken place in both cases. However, this is difficult to determine from the AERONET data alone.

These results suggest that the observed AAOD and ω_{oabs} values at Grand Forks do depend on the transport pathways of biomass smoke from their source regions to Grand Forks because these smoke particles experience physico-chemical interactions during transport. Though there are some correlations between transport time and the varying amount of absorption of the smoke plumes, merely using the spectral dependence of ω_{oabs} alone is not enough to explain the variability in absorption of the organic compounds present in the smoke. A more detailed chemical analysis (e.g., filter or aerosol mass spectrometry) is needed but is beyond the scope of this study.

ACPD
13, 32269–32289, 2013

4 Summary and conclusions

The origins of biomass smoke plumes along with their variable physico-chemical properties are reported in this study. Through an integrative analysis of collected datasets during the 2012 warm season, we briefly summarize our findings as follows:

1. Six biomass burning smoke plumes that originated from numerous wildfires in North America were observed by the newly installed Grand Forks AERONET site. The smoke plumes were transported by persistent meteorological patterns that varied in strength and location throughout the 2012 warm season (26 June–15 September). To identify the source regions, the HYSPLIT backward trajectory model was used to track these events at the 3 km level. Four out of the six cases (Cases II, III, V, and VI) had a plume transport time of approximately 24–36 h while Cases I and IV took up to 3 days.

2. The volume size distribution and spectral AOD dependence showed how each case had distinct fingerprints in terms of fine and coarse mode influences. The bimodal distributions of all six cases indicated the possibilities of coagulation and hygroscopic growth as concluded by previous studies on biomass burning aerosol transport. Specifically, Cases I and VI had the strongest coarse mode influence along with the weakest AOD spectral dependences. Case II had the strongest fine mode influence while Cases II, IV, and V had the strongest spectral AOD dependences.

3. The spectral dependences of AAOD and ω_{oabs} illustrate the varying absorption of the smoke plumes by inferring the relative contributions of strongly and weakly absorbing carbonaceous species. More specifically, the AAOD parameter is primarily influenced by aerosol particle size while ω_{oabs} is more dependent on aerosol composition. The AAOD spectral dependences for Cases I, III, and VI were weaker than those from Cases II, IV, and V. However, the spectral ω_{oabs} dependences were different in that the smoke particles in Cases III and VI had the

ACPD
13, 32269–32289, 2013

strongest absorption while Cases I, II, IV, and V had moderate to weakly absorbing particles. In addition, a weak correlation was found between plume transport time and particle absorption where strongly absorbing carbon was converted to weakly absorbing carbon.

This study takes a brief look at the evolving nature of biomass burning smoke plumes and gives a rough estimate of the absorptive properties of the smoke plumes. This can in turn aid in modeling their effects on cloud physical properties such as the first and second indirect effects which is a future area of focus for this study.

Acknowledgements. The authors wish to thank the Grand Forks AERONET PI's Jianglong Zhang, Randall Johnson, and Travis Toth. We are grateful for the help of Aaron Kennedy and Kathryn Giannecchini. We also acknowledge the MODIS mission scientists and associated NASA personnel for the production of the satellite imagery and data used in this research effort (https://earthdata.nasa.gov/labs/worldview/). We also acknowledge the NOAA scientists for the re-analysis meteorological data used in this study which is available at www.esrl.noaa.gov/psd/data/composites/day/. This research was supported by NASA EPSCoR CAN under grant NNX11AM15A at University of North Dakota.

References

Abel, S. J., Haywood, J. M., Highwood, E. J., Li, J., and Buseck, P. R.: Evolution of biomass burning aerosol properties from an agricultural fire in southern Africa, Geophys. Res. Lett., 30, 1783, doi:10.1029/2003GL017342, 2003.

Adler, G., Flores, J. M., Abo Riziq, A., Borrmann, S., and Rudich, Y.: Chemical, physical, and optical evolution of biomass burning aerosols: a case study, Atmos. Chem. Phys., 11, 1491–1503, doi:10.5194/acp-11-1491-2011, 2011.

Andreae, M. O. and Gelencsér, A.: Black carbon or brown carbon? The nature of light-absorbing carbonaceous aerosols, Atmos. Chem. Phys., 6, 3131–3148, doi:10.5194/acp-6-3131-2006, 2006.

ACPD
13, 32269–32289, 2013

Arola, A., Schuster, G., Myhre, G., Kazadzis, S., Dey, S., and Tripathi, S. N.: Inferring absorbing organic carbon content from AERONET data, Atmos. Chem. Phys., 11, 215–225, doi:10.5194/acp-11-215-2011, 2011.

Bergstrom, R. W., Pilewskie, P., Pommier, J., Rabbette, M., Russell, P. B., Schmid, B., Redemann, J., Higurashi, A., Nakajima, T., and Quinn, P. K.: Spectral absorption of solar radiation by aerosols during ACE-Asia, J. Geophys. Sci., 109, D19S15, doi:10.1029/2003JD004467, 2004.

Bergstrom, R. W., Pilewskie, P., Russell, P. B., Redemann, J., Bond, T. C., Quinn, P. K., and Sierau, B.: Spectral absorption properties of atmospheric aerosols, Atmos. Chem. Phys., 7, 5937–5943, doi:10.5194/acp-7-5937-2007, 2007.

Chung, C. E., Ramanathan, V., and Decremer, D.: Observationally constrained estimates of carbonaceous aerosol radiative forcing, P. Natl. Acad. Sci. USA, 109, 11624–11629, 2012.

Corr, C. A., Hall, S. R., Ullmann, K., Anderson, B. E., Beyersdorf, A. J., Thornhill, K. L., Cubison, M. J., Jimenez, J. L., Wisthaler, A., and Dibb, J. E.: Spectral absorption of biomass burning aerosol determined from retrieved single scattering albedo during ARCTAS, Atmos. Chem. Phys., 12, 10505–10518, doi:10.5194/acp-12-10505-2012, 2012.

Cubison, M. J., Ortega, A. M., Hayes, P. L., Farmer, D. K., Day, D., Lechner, M. J., Brune, W. H., Apel, E., Diskin, G. S., Fisher, J. A., Fuelberg, H. E., Hecobian, A., Knapp, D. J., Mikoviny, T., Riemer, D., Sachse, G. W., Sessions, W., Weber, R. J., Weinheimer, A. J., Wisthaler, A., and Jimenez, J. L.: Effects of aging on organic aerosol from open biomass burning smoke in aircraft and laboratory studies, Atmos. Chem. Phys., 11, 12049–12064, doi:10.5194/acp-11-12049-2011, 2011.

Draxler, R. R.: HYSPLIT4 user's guide, NOAA Tech. Memo. ERL ARL-230, NOAA Air Resources Laboratory, Silver Spring, MD, 1999.

Draxler, R. R. and Hess, G. D.: Description of the HYSPLIT_4 modeling system, NOAA Tech. Memo. ERL ARL-224, NOAA Air Resources Laboratory, Silver Spring, MD, 24 pp., 1997.

Draxler, R. R. and Hess, G. D.: An overview of the HYSPLIT_4 modeling system of trajectories, dispersion, and deposition, Aust. Meteor. Mag., 47, 295–308, 1998.

Draxler, R. R. and Rolph, G. D.: HYSPLIT (HYbrid Single-Particle Lagrangian Integrated Trajectory) Model access via NOAA ARL READY Website, available at: http://ready.arl.noaa.gov/HYSPLI~T.php (7 October 2013), NOAA Air Resources Laboratory, Silver Spring, MD, 2012.

Dubovik, O. and King, M.: A flexible inversion algorithm for retrieval of aerosol optical properties from Sun and sky radiance measurements, J. Geophys. Res., 105, 20673–20696, 2000.

ACPD
13, 32269–32289, 2013

Dubovik, O., Smirnov, A., Holben, B. N., Eck, T. F., King, M. D., Kaufman, Y. J., and Slutsker, I.: Accuracy assessments of aerosol optical properties retrieved from Aerosol Robotic Network (AERONET) sun and sky radiance measurements, J. Geophys. Res., 105, 9791–9806, 2000.

Gobbi, G. P., Kaufman, Y. J., Koren, I., and Eck, T. F.: Classification of aerosol properties derived from AERONET direct sun data, Atmos. Chem. Phys., 7, 453–458, doi:10.5194/acp-7-453-2007, 2007.

Holben, B. N., Eck, T. F., Slutsker, I., Smirnov, A., Sinyuk, A., Schafer, J. S., Giles, D. M., and Dubovik, O.: AERONET's version 2.0 quality assurance criteria, Remote Sensing of Atmosphere and Clouds, Proc. SPIE Int. Soc. Opt. Eng., 6408, 64080Q, doi:10.1117/12.706524, 2006.

Jacobson, M. Z.: Investigating cloud absorption effects: Global absorption properties of black carbon, tar balls, and soil dust in clouds and aerosols, J. Geophys. Res., 117, D06205, doi:10.1029/2011JD017218, 2012.

Jimenez, J. L., Canagaratna, M. R., Donahue, N. M., Prevot, A. S. H., Zhang, Q., Kroll, J. H., DeCarlo, P. F., Allan, J. D., Coe, H., Ng, N. L., Aiken, A. C., Docherty, K. S., Ulbrich, I. M., Grieshop, A. P., Robinson, A. L., Duplissy, J., Smith, J. D., Wilson, K. R., Lanz, V. A., Hueglin, C., Sun, Y. L., Tian, J., Laaksonen, A., Raatikainen, T., Rautiainen, J., Vaattovaara, P., Ehn, M., Kulmala, M., Tomlinson, J. M., Collins, D. R., Cubison, M. J., Dunlea, E. J., Huffman, J. A., Onasch, T. B., Alfarra, M. R., Williams, P. I., Bower, K., Kondo, Y., Schneider, J., Drewnick, F., Borrmann, S., Weimer, S., Demerjian, K., Salcedo, D., Cottrell, L., Griffin, R., Takami, A., Miyoshi, T., Hatakeyama, S., Shimono, A., Sun, J. Y., Zhang, Y. M., Dzepina, K., Kimmel, J. R., Sueper, D., Jayne, J. T., Herndon, S. C., Trimborn, A. M., Williams, L. R., Wood, E. C., Middlebrook, A. M., Kolb, C. E., Baltensperger, U., and Worsnop, D. R.: Evolution of organic aerosols in the atmosphere, Science, 326, 1525, doi:10.1126/science.1180353, 2009.

Kondo, Y., Matsui, H., Moteki, N., Sahu, L., Takegawa, N., Kajino, M., Zhao, Y., Cubison, M. J., Jimenez, J. L., Vay, S., Diskin, G. S., Anderson, B., Wisthaler, A., Mikoviny, T., Fuelberg, H. E., Blake, D. R., Huey, G., Weinheimer, A. J., Knapp, D. J., and Brune, W. H.: Emissions of black carbon, organic, and inorganic aerosols from biomass burning in North America and Asia in 2008, J. Geophys. Res., 116, D08204, doi:10.1029/2010JD015152, 2011.

Lack, D. A. and Cappa, C. D.: Impact of brown and clear carbon on light absorption enhancement, single scatter albedo and absorption wavelength dependence of black carbon, Atmos. Chem. Phys., 10, 4207–4220, doi:10.5194/acp-10-4207-2010, 2010.

ACPD
13, 32269–32289, 2013

Lewis, K., Arnott, W. P., Moosmüller, H., and Wold, C. E.: Strong spectral variation of biomass smoke light absorption and single scattering albedo observed with a novel dual-wavelength photoacoustic instrument, J. Geophys. Res., 113, D16203, doi:10.1029/2007JD009699, 2008.

Li, Z., Niu, F., Fan, J., Liu, Y., Rosenfeld, D., and Ding, Y.: Long-term impacts of aerosols on the vertical development of clouds and precipitation, Nat. Geosci., 4, 888–894, doi:10.1038/NGEO1313, 2011.

Logan, T., Xi, B., Dong, X., Li, Z., and Cribb, M.: Classification and investigation of Asian aerosol absorptive properties, Atmos. Chem. Phys., 13, 2253–2265, doi:10.5194/acp-13-2253-2013, 2013.

Martins, J. V., Artaxo, P., Liousse, C., Reid, J. S., Hobbs, P. V., and Kaufman, Y. J.: Effects of black carbon content, particle size, and mixing on light absorption by aerosols from biomass burning in Brazil, J. Geophys. Res., 103, 32041–32050, 1998a.

Martins, J. V., Hobbs, P. V., Weiss, R. E., and Artaxo, P.: Sphericity and morphology of smoke particles from biomass burning in Brazil, J. Geophys. Res., 103, 32051–32057, 1998b.

McKendry, I., Strawbridge, K., Karumudi, M. L., O'Neill, N., Macdonald, A. M., Leaitch, R., Jaffe, D., Cottle, P., Sharma, S., Sheridan, P., and Ogren, J.: Californian forest fire plumes over Southwestern British Columbia: lidar, sunphotometry, and mountaintop chemistry observations, Atmos. Chem. Phys., 11, 465–477, doi:10.5194/acp-11-465-2011, 2011.

Pope, C. A.: Air pollution and health – good news and bad. N. Engl. J. Med., 351, 1132–1134, 2004.

Ramanathan, V., Crutzen, P. J., Kiehl, J. T., Rosenfeld, D.: Aerosols, climate, and the hydrological cycle, Science, 294, 2119–2124, doi:10.1126/science, 2001.

Reid, J. S. and Hobbs, P. V.: Physical and optical properties of young smoke from individual biomass fires in Brazil, J. Geophys. Res., 103, 32013–32030, 1998.

Reid, J. S., Hobbs, P. V., Ferek, R. J., Blake, D. R., Martins, J. V., Dunlap, M. R., and Liousse, C.: Physical, chemical, and optical properties of regional hazes dominated by smoke in Brazil, J. Geophys. Res., 103, 32059–32080, 1998.

Reid, J. S., Koppmann, R., Eck, T. F., and Eleuterio, D. P.: A review of biomass burning emissions part II: intensive physical properties of biomass burning particles, Atmos. Chem. Phys., 5, 799–825, doi:10.5194/acp-5-799-2005, 2005.

Robock, A.: Enhancement of surface cooling due to forest fire smoke, Science, 242, 911–913, 1988.

ACPD
13, 32269–32289, 2013

Rolph, G. D.: Real-time Environmental Applications and Display sYstem (READY) Website, available at: http://ready.arl.noaa.gov (7 October 2013), NOAA Air Resources Laboratory, Silver Spring, MD, 2012.

Russell, P. B., Bergstrom, R. W., Shinozuka, Y., Clarke, A. D., DeCarlo, P. F., Jimenez, J. L., Livingston, J. M., Redemann, J., Dubovik, O., and Strawa, A.: Absorption Angstrom Exponent in AERONET and related data as an indicator of aerosol composition, Atmos. Chem. Phys., 10, 1155–1169, doi:10.5194/acp-10-1155-2010, 2010.

Schuster, G. L., Dubovik, O., and Holben, B. N.: Angstrom exponent and bimodal aerosol size distributions, J. Geophys. Res., 111, D07207, doi:10.1029/2005JD006328, 2006.

Zaveri, R. A., Shaw, W. J., Cziczo, D. J., Schmid, B., Ferrare, R. A., Alexander, M. L., Alexandrov, M., Alvarez, R. J., Arnott, W. P., Atkinson, D. B., Baidar, S., Banta, R. M., Barnard, J. C., Beranek, J., Berg, L. K., Brechtel, F., Brewer, W. A., Cahill, J. F., Cairns, B., Cappa, C. D., Chand, D., China, S., Comstock, J. M., Dubey, M. K., Easter, R. C., Erickson, M. H., Fast, J. D., Floerchinger, C., Flowers, B. A., Fortner, E., Gaffney, J. S., Gilles, M. K., Gorkowski, K., Gustafson, W. I., Gyawali, M., Hair, J., Hardesty, R. M., Harworth, J. W., Herndon, S., Hiranuma, N., Hostetler, C., Hubbe, J. M., Jayne, J. T., Jeong, H., Jobson, B. T., Kassianov, E. I., Kleinman, L. I., Kluzek, C., Knighton, B., Kolesar, K. R., Kuang, C., Kubátová, A., Langford, A. O., Laskin, A., Laulainen, N., Marchbanks, R. D., Mazzoleni, C., Mei, F., Moffet, R. C., Nelson, D., Obland, M. D., Oetjen, H., Onasch, T. B., Ortega, I., Ottaviani, M., Pekour, M., Prather, K. A., Radney, J. G., Rogers, R. R., Sandberg, S. P., Sedlacek, A., Senff, C. J., Senum, G., Setyan, A., Shilling, J. E., Shrivastava, M., Song, C., Springston, S. R., Subramanian, R., Suski, K., Tomlinson, J., Volkamer, R., Wallace, H. W., Wang, J., Weickmann, A. M., Worsnop, D. R., Yu, X.-Y., Zelenyuk, A., and Zhang, Q.: Overview of the 2010 Carbonaceous Aerosols and Radiative Effects Study (CARES), Atmos. Chem. Phys., 12, 7647–7687, doi:10.5194/acp-12-7647-2012, 2012.

ACPD
13, 32269–32289, 2013

Table 1. . A summary of the AOD, α, and α_{abs} values for the six cases. Daily AERONET data is used except for the maximum AOD_{440} values. The highest α values (> 1.7) are associated with dense smoke plumes observed over or near the vicinity of the AERONET site as evidenced by MODIS imagery (not shown). Values less than 1.7 are more correlated with hazy conditions reported near the site.

2012 warm season cases		AOD_{440} mean	AOD_{440} maximum*	α	α_{abs}
I	26 June	0.31	0.40	1.54	1.16
II	4 July	0.27	0.44	1.82	1.15
III	31 July	0.41	0.64	1.81	1.07
IV	28 August	0.41	0.52	1.84	1.13
V	30 August	0.43	0.44	1.98	1.17
VI	15 September	0.48	0.48	1.55	0.79

* Retrieved from AERONET hourly data.

ACPD
13, 32269–32289, 2013

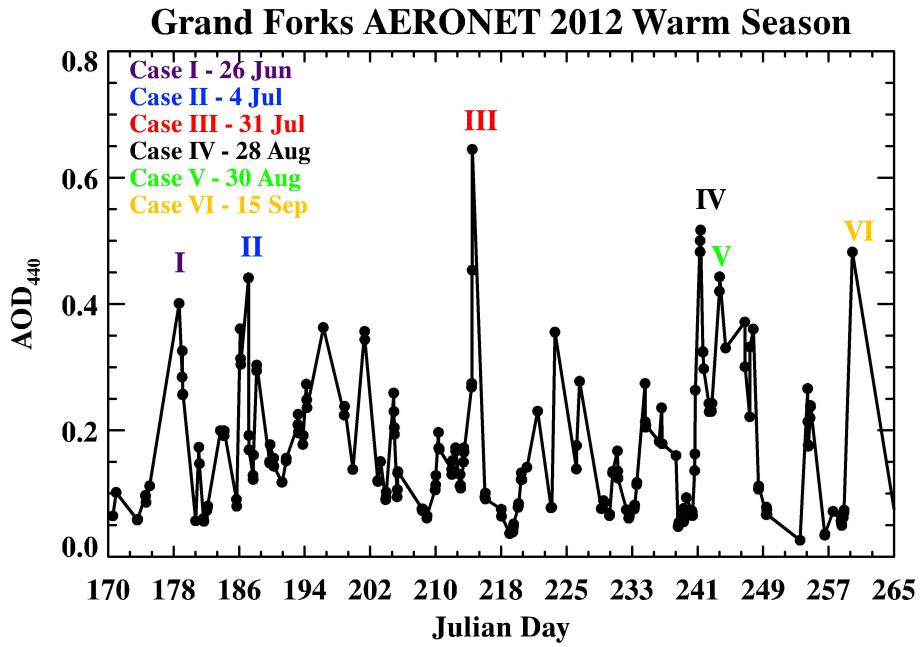

Fig. 1. Aerosol loading of smoke plumes as evidenced by the periodic increase and decrease of the hourly mean aerosol optical depth (AOD) observed by the newly installed Grand Forks AERONET site (47.91° N, 97.32° W). Each case is color coded and this convention is used in the subsequent figures.

ACPD
13, 32269–32289, 2013

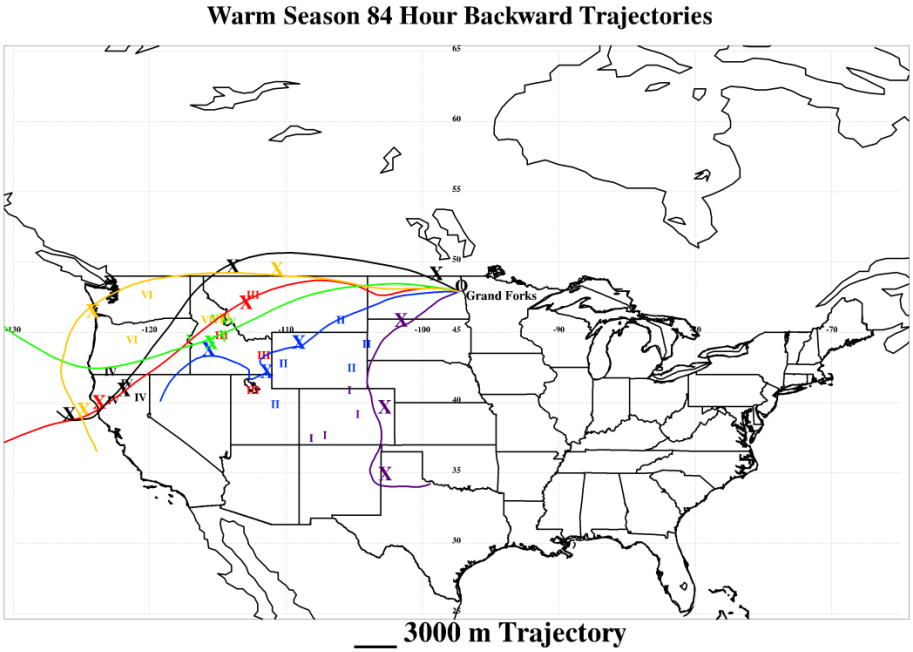

Fig. 2. HYSPLIT backward trajectories of the six cases (with the same color code as Fig. 1). The "X" characters represent a 24 h time segment of the backward trajectory that was initialized at the time of maximum aerosol loading (AOD_{440} maximum). The locations of the wildfires (roman numerals color coded by case) are identified by MODIS Aqua/Terra satellite fire products (http://earthdata.nasa.gov/data/near-real-time-data/data/hazards-and-disasters/fires).

ACPD
13, 32269–32289, 2013

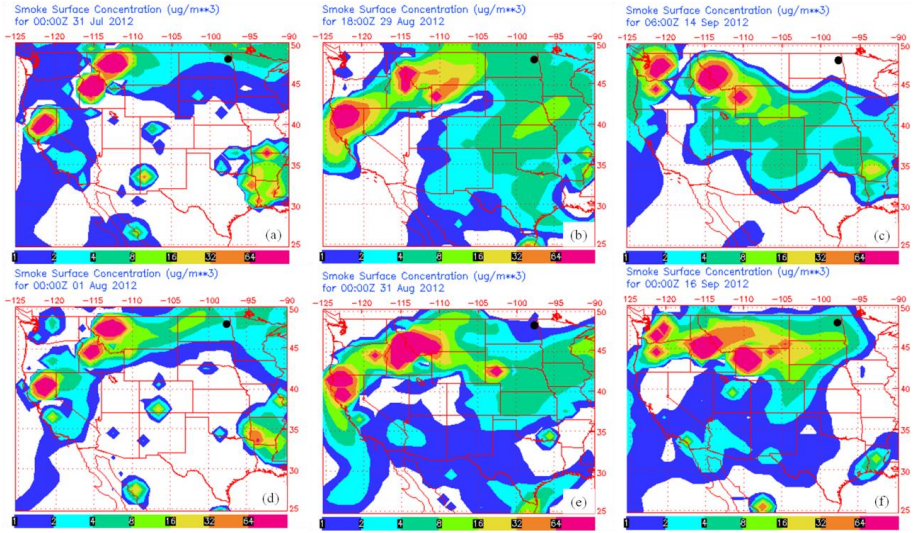

Fig. 3. Locations of the wildfire source regions for Cases **(a)** III, **(b)** V, and **(c)** VI while **(d)**, **(e)**, and **(f)** show the smoke plumes for the respective cases over Grand Forks (black circle).

ACPD
13, 32269–32289, 2013

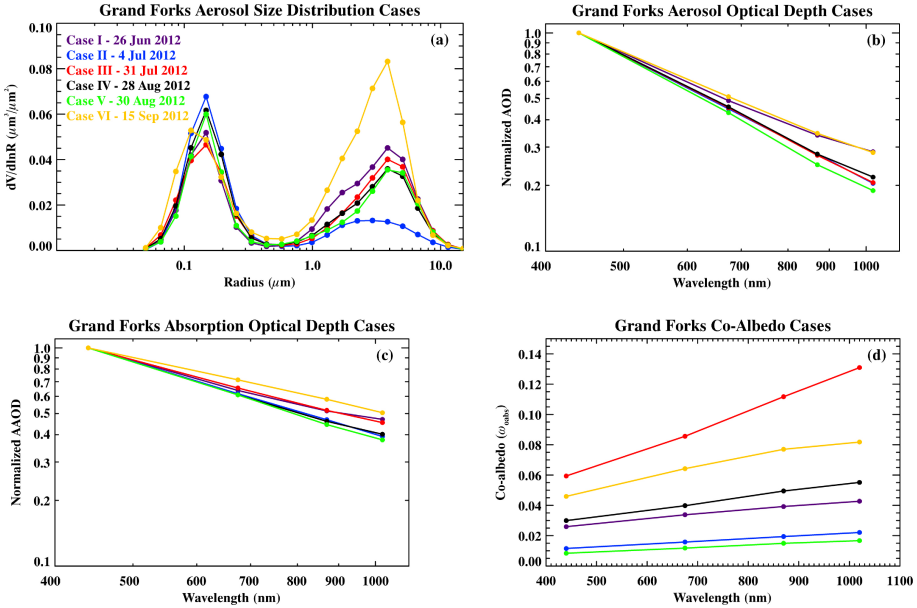

Fig. 4. (a) Particle volume size distribution, the spectral dependences of **(b)** AOD, **(c)** AAOD, and **(d)** ω_{oabs} for the six selected cases.

ACPD
13, 32269–32289, 2013

Biomass burning aerosol properties over the Northern Great Plains

T. Logan et al.